Theor Chem Acc (2011) 129:331–342
DOI 10.1007/s00214-010-0819-2

REGULAR ARTICLE

Time-dependent density functional theory gradients in the Amsterdam density functional package: geometry optimizations of spin-flip excitations

Michael Seth · Grzegorz Mazur · Tom Ziegler

Received: 1 June 2010 / Accepted: 9 September 2010 / Published online: 25 September 2010

Abstract An implementation of time-dependent density functional theory (TDDFT) energy gradients into the Amsterdam density functional theory program package (ADF) is described. The special challenges presented by Slater-type orbitals in quantum chemical calculation are outlined with particular emphasis on details that are important for TDDFT gradients. Equations for the gradients of spin-flip TDDFT excitation energies are derived. Example calculations utilizing the new implementation are presented. The results of standard calculations agree well with previous results. It is shown that starting from a triplet reference, spin-flip TDDFT can successfully optimize the geometry of the four lowest singlet states of CH_2 and three other isovalent species. Spin-flip TDDFT is used to calculate the potential energy curve of the breaking of the C–C bond of ethane. The curve obtained is superior to that from a restricted density functional theory calculation, while at the same time the problems with spin contamination exhibited by unrestricted density functional theory calculations are avoided.

Keywords Time-dependent density functional theory · Analytical gradients · Slater-type orbitals · Spin-flip

Dedicated to Professor Pekka Pyykkö on the occasion of his 70th birthday and published as part of the Pyykkö Festschrift Issue.

M. Seth (✉) · T. Ziegler
Department of Chemistry, University of Calgary,
2500 University Drive NW, Calgary, AB T2N 1N4, Canada
e-mail: mseth@ucalgary.ca

G. Mazur
Department of Computational Methods in Chemistry,
Jagiellonian University, Ingardena 3, 30-060 Kraków, Poland

1 Introduction

In recent years, linear response time-dependent density functional theory (LR-TDDFT) [1–5] has become the most popular formalism for calculating excitation energies of molecules. LR-TDDFT, which we shall further abbreviate to TDDFT, produces results that are accurate enough to be useful at a reasonable computational cost. It does have some limitations. In combination with a linear response and a frequency-independent kernel (the adiabatic approximation), only transitions that are well-described by single excitations can be treated. Even certain types of transitions that are often considered to be single excitations, such as long-range charge-transfer transitions, have also been found to be troublesome. Overcoming these difficulties is an area of active research. Despite these challenges, it has been shown that TDDFT can provide predictions of vertical excitation energies of good accuracy in a wide range of areas of application [5]. Moving beyond vertical excitation energies, the applicability of TDDFT has been extended further by the advent of analytic derivatives of the excitation energy.

The first implementation of TDDFT gradients was described by Van Caillie and Amos [6, 7]. They obtained the derivative of the excitation energy (ω) with respect to a perturbation by the straightforward differentiation of the TDDFT equations. Furche and Ahlrichs provided an elegant alternative formulation by applying a Lagrangian-based approach [8–10]. These two treatments assumed a real perturbation. We will focus on this type of perturbation in this work, but we note that TDDFT in the presence of an imaginary perturbation like a magnetic field or spin-orbit coupling is also an area of interest [11, 12].

Perhaps, the most important perturbation that can be considered in the context of a molecule is the motion of a

nucleus. The availability of all first derivatives of ω with respect to nuclear motion opens up the possibility of exploring the potential energy surface (PES) of excited states. In the case of the ground state, the most common applications of nuclear gradients involve the location of extrema such as local minima (stable geometries) and first-order saddle points (transition states). Furthermore, these extrema can be characterized using second derivatives of the energy obtained analytically or through numerical differentiation of the first derivatives.

Nuclear gradients of the excitation energy can be used to perform the same tasks for excited states. Near the equilibrium geometry, the ground state of a molecule is often well isolated from other states, particularly if that state represents a closed-shell electron configuration. Excited states are generally less isolated, and features that appear when two PES come close to each other, such as avoided crossings and conical intersections, become more prevalent. Recent studies have considered how well TDDFT can characterize such features [13–17]. While some successes have been reported, some difficulties have been encountered because of the inability of TDDFT calculations to describe the doubly excited states that are often important in the region of conical intersections [13].

The implementations of TDDFT gradients described by Van Caillie and Amos and Furche and Ahlrichs are based upon program codes that utilize Gaussian type orbitals (GTOs). GTOs are the most popular form of basis function for describing molecular orbitals because the analytic evaluation of two-electron integrals is relatively straightforward. TDDFT gradients in combination with plane wave basis functions have been presented by Hutter [18, 19].

Slater-type orbitals (STOs) provide an alternative to GTOs. The radial behavior of STOs near a nucleus follows more closely that of exact orbitals, meaning that fewer STOs are required to describe a given molecule. The challenge of two-electron integrals has been overcome [20–23], and several STO-based quantum chemistry codes have been developed that are competitive with programs based on other types of basis function. These codes can perform TDDFT calculations [24, 25], but as far as we are aware, no implementation of TDDFT gradients in a STO-based code has been presented. The first topic discussed in this paper will be our implementation of TDDFT gradients in the STO-based Amsterdam density functional (ADF) program. This implementation has significant overlap with the GTO-based formalism, and we shall therefore focus on the special challenges created by STOs.

A feature of the TDDFT implementation in ADF is the possibility of performing spin-flip TDDFT (SF-TDDFT) calculations. In a conventional TDDFT calculation, only $\alpha - \alpha$ or $\beta - \beta$ excitations are possible and the m_s quantum number is conserved ($\Delta m_s = 0$). The coupling matrix used in TDDFT to evaluate excitation energies and transition densities is assumed to be diagonal in spin. Off-diagonal terms in the coupling matrix allow transitions made up of excitations where a spin is flipped ($\alpha - \beta, \Delta m = -1$ or $\beta - \alpha$, $\Delta m = +1$) to be described. In 2003 Shao, Head-Gordon and Krylov showed that starting from a standard formulation of TDDFT, contributions to the off-diagonal part of the coupling matrix could only come from exact exchange [26]. It was found that an admixture of exact exchange rather larger than that used in most applications was needed to obtain reasonable results. In 2004, Wang and Ziegler [27, 28] showed that the exchange-correlation term in the coupling matrix also can contribute to the off-diagonal terms if one starts with a noncollinear form of the exchange-correlation potential [29–31]. In this treatment, any functional can provide nonzero coupling terms that cause spin-flips.

In their original work, Shao, Head-Gordon and Krylov included SF-TDDFT gradients. The second topic that we shall discuss is an implementation of SF-TDDFT gradients in the Wang-Ziegler formulation.

In the last part of this paper, a few example calculations performed with our implementation will be described. To begin with, several calculations involving small molecules will be presented to demonstrate that a STO-based TDDFT-gradients program can produce results comparable to other codes. The remaining examples will showcase the possibilities of spin-flip gradients with examples in two areas where SF-TDDFT can be very useful. These are describing excited states that are doubly excited with respect to the ground state as well as the dissociation of a single bond into two radicals.

2 Theory

For the most part, the notation used here will follow that presented by Furche and Ahlrichs [8]. A molecular orbital will be indicated by the symbol ϕ with the subscripts a, b, c..., indicating a MO that is unoccupied in the ground state, i, j, k... indicate an orbital that is occupied in the ground state and p, q, r... indicate any orbital. Greek subscripts $\sigma, \tau, \upsilon \ldots$ are spin indices. A basis function will be denoted by χ and subscripted μ, ν, κ.... The superscript ξ indicates differentiation with respect to a real perturbation. A superscript ξ inside brackets indicates that only contributions from explicit differentiation of the basis functions are included. In general, multiple integral signs and r, r', dr and dr' symbols will be neglected in the one- and two-electron integrals to simplify the notation.

2.1 DFT with STOs

As was noted in the introduction, the analytical evaluation of two-electron integrals over STOs is very difficult. In this section, we will briefly review how this problem is dealt with in the ADF program [32–34] with an emphasis on issues that are relevant to TDDFT gradients.

Two or three different types of two-electron integral are encountered in most DFT calculations. Firstly, integrals over the local part of the exchange-correlation functional need to be evaluated. Since the functional is local, these integrals can easily be evaluated numerically. This is the approach taken by almost all DFT codes, including ADF.

The second type of integral, Coulomb integral, is calculated in ADF by a combination of numerical integration and fitting. A Coulomb interaction between two densities ρ^1 and ρ^2 can be written as

$$E_c = \iint \frac{\rho^1(r)\rho^2(r')}{|r-r'|}\mathrm{d}r\mathrm{d}r' \tag{1}$$

In order to make it possible to evaluate such an integral numerically, the Coulomb potential due to one of the densities is fit in a suitable basis [20] to give a fit potential

$$\rho^1 \approx \sum_k a_k f_k \tag{2}$$

$$V_C^1 = \sum_k a_k J_k \tag{3}$$

$$J_k(r) = \int \frac{f_k(r')}{|r-r'|}\mathrm{d}r \tag{4}$$

where f_k and a_k are fit functions and fit coefficients. Equation 1 becomes

$$E_c = \int V_C^1(r)\rho_2(r)\mathrm{d}r \tag{5}$$

an integral that can be evaluated numerically in a straightforward manner.

The third type of two-electron interaction is that provided by exact exchange. In this case, a local potential cannot be obtained through density fitting. Instead, the individual integrals over AOs are considered directly. A given integral $(\mu\nu|\lambda\kappa)$

$$(\mu\nu|\lambda\kappa) = \iint \chi_\mu(r)\chi_\nu(r)\frac{1}{|r-r'|}\chi_\lambda(r')\chi_\kappa(r')\mathrm{d}r\mathrm{d}r' \tag{6}$$

where χ is a Slater-type function, is evaluated by fitting the density produced by each of the pairs of basis functions [21, 23]

$$\chi_\mu(r)\chi_\nu(r) = \sum_i a_i^{\mu\nu} f_{AB,i} \tag{7}$$

$$\chi_\lambda(r)\chi_\kappa(r) = \sum_i a_i^{\lambda\kappa} f_{CD,i} \tag{8}$$

The subscript AB (CD) indicates that a function is included in the fit only if it is centered on the same atom as basis function χ_μ or χ_ν (χ_λ or χ_κ). The final expression for the two-electron integral is

$$(\mu\nu|\lambda\kappa) = \sum_{ij} a_i^{\mu\nu} a_j^{\lambda\kappa} (f_{AB,i}|f_{CD,j}) \tag{9}$$

and $(f_{AB,i}|f_{CD,j})$ can be evaluated analytically.

Numerical integration obviously plays a central role in the ADF program. The way in which a grid for the integration is produced and the fineness of that grid will strongly influence the quality of any results obtained. Grids are produced by a method that takes advantage of the structural features common to all densities that correspond to a molecule [35, 36]. Even with this specialized approach, stable evaluation of the Coulomb energies of the density of a molecule can be problematic as that density will have very large values and gradients near the nuclei. This problem can be avoided by firstly dividing the density into two parts

$$\rho_1 = \sum_A \rho_A + \Delta\rho_1 \tag{10}$$

where A runs over all nuclei in the molecule, ρ_A is the spherical density corresponding to the isolated atom A and $\Delta\rho$ is the change in density required to make up the total molecular density. The Coulomb potential due to a density can be divided in a similar manner

$$V_C^1 = \sum_A V_C^A + \Delta V_C^2 \tag{11}$$

For the Coulomb interaction between ρ_1 and ρ_2, the terms that are responsible for the numeric instability terms have the form $\int V_C^A \rho^A$. Here, both the density and potential can be very large at the same grid point, which might lead to significant numerical errors. The contribution of these terms to the Coulomb energy is constant irrespective of the form of the densities ρ_1 and ρ_2 or the positions of the nuclei [37, 38]. The derivative of $\int V_C^A \rho^A$ with respect to nuclear motion is zero. Relative energies are the important quantities in chemistry. Since the $\int V_C^A \rho^A$ terms are constant, they can be chosen to be zero avoiding numerical instability. Thus, provided that $\Delta\rho$ is not too large, which is typically the case when ρ_1 is the electron density of a molecule, dividing the density according to Eq. 10 should ensure numerically stable Coulomb energies.

2.2 TDDFT with ADF

In a TDDFT calculation of molecular excitation energies, the equation to be solved is [2]

$$\omega \begin{pmatrix} 1 & 0 \\ 0 & -1 \end{pmatrix} \begin{pmatrix} X \\ Y \end{pmatrix} = \begin{pmatrix} \mathrm{A} & \mathrm{B} \\ \mathrm{B}^* & \mathrm{A}^* \end{pmatrix} \begin{pmatrix} X \\ Y \end{pmatrix} \tag{12}$$

where ω is interpreted as the energy difference between the reference state and another state and X and Y describe the transition density between the two states.

If all orbitals obtained from the Kohn–Sham equations can be chosen to be real Eq. 12 can be converted into a form that is more useful for our current purposes

$$\omega = \frac{1}{2}\big((X^\dagger + Y^\dagger)(\mathrm{A}+\mathrm{B})(X+Y) + (X^\dagger - Y^\dagger)(\mathrm{A}-\mathrm{B})(X-Y)\big) \tag{13}$$

In a conventional TDDFT calculation

$$A_{ai\sigma,bj\tau} + B_{ai\sigma,bj\tau} = \delta_{\sigma\tau}\delta_{ab}\delta_{ij}(\varepsilon_{b\tau} - \varepsilon_{j\tau}) + K^S_{ai\sigma,bj\tau} \tag{14}$$

$$A_{ai\sigma,bj\tau} - B_{ai\sigma,bj\tau} = \delta_{\sigma\tau}\delta_{ab}\delta_{ij}(\varepsilon_{b\tau} - \varepsilon_{j\tau}) + K^A_{ai\sigma,bj\tau} \tag{15}$$

The superscripts S and A indicate that one coupling matrix matrix is symmetric with respect to permutation of a and i (or b and j), while the other matrix is anti-symmetric.

$$K^S_{ai\sigma,bj\tau} = 2(ai\sigma|bj\tau) + 2\big(ai\sigma|f^{xc}_{\sigma\tau}|bj\tau\big) - \delta_{\sigma\tau}c_X((ab\sigma|ij\tau) + (aj\sigma|bi\tau)) \tag{16}$$

$$K^A_{ai\sigma,bj\tau} = -\delta_{\sigma\tau}c_X((ab\sigma|ij\tau) - (aj\sigma|bi\tau)) \tag{17}$$

where $(ai\sigma|bj\tau)$ is a two-electron integral over MOs defined similarly to the integral over AOs (Eq. 6). The coefficient c_X corresponds to the fraction of exact exchange included in the chosen functional. The term $f^{xc}_{\sigma\tau}$ is the exchange-correlation kernel. In ADF, this is generally the frequency-independent kernel corresponding to the VWN5 LDA functional [39] irrespective of what functional is used to derive the orbitals (the adiabatic local-density approximation, ALDA) [40]. In this case,

$$f^{xc,ALDA}_{\sigma\tau} = \frac{\delta^2 E^{xc}_{VWN5}}{\delta\rho_\sigma\delta\rho_\tau} \tag{18}$$

If the functional used to obtain the reference MOs includes exact exchange, the contribution to the K^S matrix from f^{xc} is attenuated by a factor of $(1 - c_X)$ under the ALDA approximation.

As we shall see shortly, the use of the ALDA approximation both simplifies and complicates the evaluation of TDDFT gradients.

If the reference state is closed-shell, the K-matrices just described correspond to singlet–singlet excitations. It is also possible to evaluate singlet–triplet excitations with the choice of

$$K^S_{ai\sigma,bj\tau} = 2\Big(ai\sigma|f^{xc,ALDA}_{ST,\sigma\tau}|bj\tau\Big) - \delta_{\sigma\tau}c_X((ab\sigma|ij\tau) + (aj\sigma|bi\tau)) \tag{19}$$

$$K^A_{ai\sigma,bj\tau} = -\delta_{\sigma\tau}c_X((ab\sigma|ij\tau) - (aj\sigma|bi\tau)) \tag{20}$$

$$f^{xc,ALDA}_{ST,\sigma\tau} = \delta_{\sigma\tau}(1-c_X)\frac{1}{2}\left(\frac{\delta^2 E^{xc}}{\delta\rho_\alpha\delta\rho_\alpha} + \frac{\delta^2 E^{xc}}{\delta\rho_\beta\delta\rho_\beta} - 2\frac{\delta^2 E^{xc}}{\delta\rho_\alpha\delta\rho_\beta}\right) \tag{21}$$

Following the discussion in Sect. 2.1, we write Eq. 13 in a form that more closely reflects how it is calculated in ADF

$$\begin{aligned}\omega = \frac{1}{2}\Bigg(&\sum_{ai\sigma}((X+Y)_{ai\sigma}(X+Y)_{ai\sigma} + (X-Y)_{ai\sigma}(X-Y)_{ai\sigma})(\varepsilon_{a\sigma} - \varepsilon_{i\sigma}) \\ &+ 2\sum_\sigma \int \rho^{X+Y}_\sigma V^{X+Y}_C + 2(1-c_X) \\ &\times \sum_{\sigma\tau}\int \rho^{X+Y}_\sigma f^{xc,ALDA}_{\sigma\tau}\rho^{X+Y}_\tau \\ &- c_X \sum_{ai\sigma,bj\sigma}\big((X+Y)_{ai\sigma}(X+Y)_{ai\sigma}((ab\sigma|ij\tau) + (aj\sigma|bi\tau)) \\ &+ (X-Y)_{ai\sigma}(X-Y)_{ai\sigma}((ab\sigma|ij\tau) - (aj\sigma|bi\tau))\big)\Bigg)\end{aligned} \tag{22}$$

where ρ^{X+Y}_σ is the density obtained from the vector $(X+Y)$ corresponding to spin σ

$$\rho^{X+Y}_\sigma = \sum_{\mu\nu}(X+Y)_{\mu\nu\sigma}\chi_\mu\chi_\nu \tag{23}$$

and V^{X+Y}_C is the Coulomb potential obtained from a fit of that density summed over spin.

Equation 22 can be converted into the equation for singlet–triplet excitations by using $f^{xc,ALDA}_{ST,\sigma\tau}$ and neglecting the $\rho^{X+Y}_\sigma V^{X+Y}_C$ term.

2.2.1 SF-TDDFT

In the Wang-Ziegler formulation of spin-flip excitations [27, 28], only the exchange-correlation kernel contributes to the coupling matrix. The $\mathrm{A}+\mathrm{B}$ and $\mathrm{A}-\mathrm{B}$ matrices have the following form if the spin quantization of the reference orbitals is collinear and quantized along the z-axis.

$$A_{ai\sigma,bj\tau} + B_{ai\sigma,bj\tau} = \delta_{\sigma\tau}\delta_{ab}\delta_{ij}\big(\varepsilon_{b\sigma'} - \varepsilon_{j\sigma}\big) + K^{SF,S}_{ai\sigma,bj\tau} \tag{24}$$

$$A_{ai\sigma,bj\tau} - B_{ai\sigma,bj\tau} = \delta_{\sigma\tau}\delta_{ab}\delta_{ij}\big(\varepsilon_{b\sigma'} - \varepsilon_{j\sigma}\big) + K^{SF,A}_{ai\sigma,bj\tau} \tag{25}$$

$$K^{SF,S}_{ai\sigma,bj\tau} = \delta_{\sigma\tau}\Big(a\sigma' i\sigma\Big|f^{xc,ALDA}_{SF,\sigma\tau}\Big|b\tau' j\tau\Big) + \Big(a\sigma' i\sigma\Big|f^{xc,ALDA}_{SF,\sigma\tau}\Big|j\tau' b\tau\Big) \tag{26}$$

$$K^{SF,A}_{ai\sigma,bj\tau} = \delta_{\sigma\tau}\Big(a\sigma' i\sigma\Big|f^{xc,ALDA}_{SF,\sigma\tau}\Big|b\tau' j\tau\Big) - \Big(a\sigma' i\sigma|f^{xc,ALDA}_{SF,\sigma\tau}|j\tau' b\tau\Big) \tag{27}$$

$$f_{SF,\sigma\tau}^{xc,ALDA} = \delta_{\sigma\tau}\frac{1}{\rho_\alpha - \rho_\beta}\left(\frac{\delta E^{xc}}{\delta\rho_\alpha} - \frac{\delta E^{xc}}{\delta\rho_\beta}\right) \tag{28}$$

where $\sigma \neq \sigma'$ and $\tau \neq \tau'$.

The SF-TDDFT equation equivalent to Eq. 22 is

$$\begin{aligned}\omega = \frac{1}{2}\Bigg(&\sum_{ai\sigma}\big((X+Y)_{a\sigma' i\sigma}(X+Y)_{a\sigma' i\sigma} \\ &+(X-Y)_{a\sigma' i\sigma}(X-Y)_{a\sigma' i\sigma}\big)(\varepsilon_{a\sigma'} - \varepsilon_{i\sigma}) \\ &+2\sum_{\sigma\tau}\int \rho_\sigma^{X+Y} f_{SF,\sigma\tau}^{xc,ALDA}\rho_\tau^{X+Y}\Bigg)\end{aligned} \tag{29}$$

where ρ_σ^{X+Y} is now the density obtained from the vector $(X+Y)$ corresponding to the spin-flip $\sigma \to \sigma'$.

2.3 TDDFT gradients

The formulations of TDDFT derivatives presented by Van Caillie and Amos and Furche and Ahlrichs utilize AO integrals and their derivatives [6–9]. Their equation for ω^ξ is

$$\begin{aligned}\omega^\xi = &\sum_{\mu\nu\sigma} h_{\mu\nu}^\xi P_{\mu\nu\sigma} + \sum_{\mu\nu\sigma} V_{\mu\nu\sigma}^{xc(\xi)} P_{\mu\nu\sigma} \\ &+ \sum_{\mu\nu\kappa\lambda\sigma\tau}(\mu\nu|\kappa\lambda)^\xi \Gamma_{\mu\nu\sigma\kappa\lambda\tau} \\ &+ \sum_{\mu\nu\kappa\lambda\sigma\tau} f_{\mu\nu\sigma\kappa\lambda\tau}^{xc(\xi)}(X+Y)_{\mu\nu\sigma}(X+Y)_{\kappa\lambda\tau} \\ &- \sum_{\mu\nu\sigma} S_{\mu\nu}^\xi W_{\mu\nu\sigma}\end{aligned} \tag{30}$$

where $h_{\mu\nu}^\xi$, $(\mu\nu|\kappa\lambda)^\xi$ and $S_{\mu\nu}^\xi$ are derivatives of one-electron, two-electron and overlap AO integrals, respectively, $V_{\mu\nu}^{xc(\xi)}$ and $f_{\mu\nu\sigma\kappa\lambda\tau}^{xc(\xi)}$ are the explicit derivatives of the exchange-correlation potential and kernel. P is the relaxed one-particle difference density matrix.

A form of Eq. 30 suitable for a STO-based TDDFT code is

$$\begin{aligned}\omega^\xi = &\sum_\sigma \int \rho_\sigma^{P(\xi)}\left(T + V_{ext} + V_C + V_\sigma^{xc}\right) \\ &+ \sum_\sigma \int \left(V_C^P \rho_\sigma^{(\xi)} + V_{ext}^\xi \rho_\sigma^P\right) + \sum_{\sigma\tau}\int \rho_\sigma^P f_{\sigma,\tau}^{xc,FULL}\rho_\tau^{(\xi)} \\ &+ \sum_{\sigma\tau}\int \rho_\sigma^{(X+Y)(\xi)}\left(V_C^{(X+Y)} + f_{SS,\sigma\tau}^{xc,ALDA}\rho_\tau^{(X+Y)}\right) \\ &+ \sum_{\sigma\tau\upsilon}\int \rho_\sigma^{(X+Y)}\rho_\tau^{(X+Y)}\rho_\upsilon^{(\xi)} g_{\sigma\tau\upsilon}^{xc,ALDA} \\ &+ \sum_{\mu\nu\kappa\lambda\sigma\tau}(\mu\nu|\kappa\lambda)^\xi \Gamma_{\mu\nu\sigma\kappa\lambda\tau}^X - \sum_{\mu\nu\sigma} S_{\mu\nu}^{(\xi)} W_{\mu\nu\sigma}\end{aligned} \tag{31}$$

where $\Gamma_{\mu\nu\sigma\kappa\lambda\tau}^X$ is the part of the two-electron derivative coefficient (Eq. 27, Ref. [8]) that comes from exact exchange and $(\mu\nu|\kappa\lambda)^\xi$ is the derivative of a fit two-electron integral. The potential V_{ext} includes the potential due to the nuclei and any other external perturbation. ρ is the density of the reference, ρ^{X+Y} is the transition density defined in Eq. 23, and ρ^P is the relaxed one-particle difference density

$$\rho_\sigma^P = \sum_{\mu\nu} P_{\mu\nu\sigma}\chi_\mu\chi_\nu \tag{32}$$

$$P = T + Z \tag{33}$$

$$\begin{aligned}T_{ij\sigma} = -\frac{1}{2}\sum_a &\big((X+Y)_{ai\sigma}(X+Y)_{aj\sigma} \\ &+ (X-Y)_{ai\sigma}(X-Y)_{aj\sigma}\big)\end{aligned} \tag{34}$$

$$\begin{aligned}T_{ab\sigma} = \frac{1}{2}\sum_i &\big((X+Y)_{ai\sigma}(X+Y)_{bi\sigma} \\ &+(X-Y)_{ai\sigma}(X-Y)_{bi\sigma}\big)\end{aligned} \tag{35}$$

$$T_{ai\sigma} = T_{ia\sigma} = 0 \tag{36}$$

$$Z_{ab\sigma} = Z_{ij\sigma} = 0 \tag{37}$$

the occupied-virtual elements of Z are from the solution of the equation

$$(\mathrm{A}+\mathrm{B})Z = R \tag{38}$$

The single Eq. 38 is solved in place of the $3N$ coupled-perturbed Kohn–Sham equations [41]. The elements of $(\mathrm{A}+\mathrm{B})$ are as defined in Eqs. 14–17 except that the ALDA approximation should not be applied. The exchange-correlation kernel in this case must be that derived from the functional chosen to calculate the reference state orbitals. To distinguish this kernel from $f^{xc,ALDA}$, we denote it as $f^{xc,FULL}$. Expressions for $f^{xc,FULL}$ that cover many of the available functionals can be found in the Appendix of [42].

R is given by

$$\begin{aligned}R_{ai\sigma} = &\sum_b\big\{(X+Y)_{bi\sigma}H_{ab\sigma}^+[X+Y] \\ &+ (X-Y)_{bi\sigma}H_{ab\sigma}^-[X-Y]\big\} \\ &+ \sum_j\Big\{(X+Y)_{aj\sigma}H_{ij\sigma}^+[X+Y] \\ &+ (X-Y)_{aj\sigma}H_{ij\sigma}^-[X-Y]\Big\} + H_{ai\sigma}^+[T] \\ &+ 2\sum_{\tau\upsilon}\int \phi_{a\sigma}\phi_{i\sigma}\rho_\tau^{X+Y}\rho_\upsilon^{X+Y} g_{\sigma\tau\upsilon}^{xc,ALDA}\end{aligned} \tag{39}$$

where

$$\begin{aligned}H_{pq\sigma}^+[M] = &2\int \phi_{p\sigma}\phi_{q\sigma}\left(V_C^M + \sum_\tau f_{\sigma\tau}^{xc}\rho_\tau^M\right) \\ &- \sum_{rs\tau} c_X\delta_{\sigma\tau}[(pr\sigma|sq\sigma) + (ps\sigma|rq\sigma)]M_{rs\sigma}\end{aligned} \tag{40}$$

$$H^{-}_{pq\sigma}[M] = -\sum_{rs\tau} c_X \delta_{\sigma\tau}[(pr\sigma|sq\sigma) - (ps\sigma|rq\sigma)]M_{rs\sigma} \quad (41)$$

Here, the full kernel is needed when $M = T, P$, and the ALDA kernel is required when $M = X + Y$.

The final term in Eq. 39 that includes the third-order functional derivative g^{xc} is considerably simplified by the ALDA approximation. For standard and singlet–triplet excitations, we have

$$g^{xc,ALDA}_{SS,\sigma\tau\upsilon} = \frac{\delta^3 E_{xc}}{\delta\rho_\sigma \delta\rho_\tau \delta\rho_\upsilon} \quad (42)$$

$$g^{xc,ALDA}_{ST,\sigma\tau\upsilon} = \delta_{\sigma\tau}\frac{1}{2}\left(\frac{\delta^3 E_{xc}}{\delta\rho_\alpha \delta\rho_\alpha \delta\rho_\upsilon} + \frac{\delta^3 E_{xc}}{\delta\rho_\beta \delta\rho_\beta \delta\rho_\upsilon} - 2\frac{\delta^3 E_{xc}}{\delta\rho_\alpha \delta\rho_\beta \delta\rho_\upsilon}\right) \quad (43)$$

The matrix that determines the contribution to ω^ξ from the derivatives of overlap integral is

$$\begin{aligned} W_{ij\sigma} = &\sum_a \omega\Big\{((X+Y)_{ai\sigma}(X-Y)_{aj\sigma} \\ &+ (X-Y)_{ai\sigma}(X+Y)_{aj\sigma}) \\ &- \sum_a \varepsilon_{a\sigma}((X+Y)_{aj\sigma}(X+Y)_{ai\sigma} \\ &+ (X-Y)_{aj\sigma}(X-Y)_{ai\sigma})\Big\} \\ &+ H^{+}_{ij\sigma}[P] + 2\sum_{\tau\upsilon}\int \phi_{i\sigma}\phi_{j\sigma}\rho^{(X+Y)}_\tau \rho^{(X+Y)}_\upsilon g^{xc,ALDA}_{\sigma\tau\upsilon} \end{aligned} \quad (44)$$

$$\begin{aligned} W_{ab\sigma} = &\sum_i \omega\Big\{((X+Y)_{ai\sigma}(X-Y)_{bi\sigma} + (X-Y)_{ai\sigma}(X+Y)_{bi\sigma}) \\ &+ \sum_i \varepsilon_{i\sigma}((X+Y)_{ai\sigma}(X+Y)_{bi\sigma} + (X-Y)_{ai\sigma}(X-Y)_{bi\sigma})\Big\} \end{aligned} \quad (45)$$

$$\begin{aligned} W_{ia\sigma} = Z_{ai\sigma}\varepsilon_{i\sigma} + \sum_j \Big\{&(X+Y)_{aj\sigma}H^{+}_{ji\sigma}[X+Y] \\ &+ (X-Y)_{aj\sigma}H^{-}_{ji\sigma}[X-Y]\Big\} \end{aligned} \quad (46)$$

In deriving Eq. 31, use was made of the identities

$$\sum_\sigma \int V^{xc(\xi)}_\sigma \rho^P_\sigma = \sum_{\sigma\tau}\int f^{xc,FULL}_{\sigma\tau}\rho^P_\sigma \rho^{(\xi)}_\tau \quad (47)$$

$$\sum_{\sigma\tau}\int \rho^{X+Y}_\sigma f^{xc,ALDA(\xi)}_{\sigma\tau}\rho^{X+Y}_\tau = \sum_{\sigma\tau\upsilon}\int \rho^{X+Y}_\sigma g^{xc,ALDA}_{\sigma\tau\upsilon}\rho^{X+Y}_\tau \rho^{(\xi)}_v \quad (48)$$

It was noted in Sect. 2.1 that the accuracy of Coulomb energies evaluated by numerical integration was poor unless the density was divided into atomic and relaxation contributions and the large, constant but numerically unstable, portion of the integral near the nucleus was set to zero. Further to that discussion, we mention two points that are relevant to the present subject. Firstly, the error in the integral (Eq. 5) was due to the density part of the integrand as the Coulomb potential was smoothed out by the fitting process. Secondly, the densities ρ^P and ρ^{X+Y} are unlikely to cause numerical instability. These densities correspond to differences in density between occupied valence and low-lying virtual orbitals, which should not be particularly large at any point in space. Given these considerations, if the perturbation ξ represents the motion of a nucleus, only the second term in Eq. 31 will be problematic. The accuracy of this Coulomb term was ensured by partitioning $\rho^{(\xi)}$ as in Eq. 10 and making use of translational invariance. If ξ corresponds to moving nucleus A in direction X, the problematic term can then be written as

$$\sum_\sigma \int \left(V^P_C \rho^{(\xi)}_\sigma + \rho^P_\sigma V^\xi_{ext}\right)$$

$$= \sum_\sigma \int \left(V^P_C \Delta\rho^{(\xi)}_\sigma + V^P_C \rho^{(\xi)}_A + \rho^P_\sigma V^\xi_N\right) \quad (49)$$

$$= \sum_\sigma \left(V^P_C \Delta\rho^{(\xi)}_\sigma - \frac{d\rho^P_\sigma}{dX}\left(V^A_C + V^A_N\right)\right) \quad (50)$$

where V^A_C and V^A_N are the Coulomb and nuclear potentials of the isolated atom A. The nuclear potential is included here because combining it with the isolated atom Coulomb potential further improves numerical stability. The Coulomb term can also be calculated accurately by evaluating it as $\int V^{(\xi)}_C \rho^P$. However, this approach would require $3N$ density fits for each iteration of a geometry optimization, making it prohibitively expensive.

As was noted by Furche and Ahlrichs [8], if, rather than the motion of a nucleus, ξ corresponds to some other real perturbation that does not modify the basis functions, then the formalism is simplified considerably. In this case, only the $\int V^\xi_{ext}\rho^P$ term from Eq. 31 is nonzero. ρ^P then can be used to calculate the change in the appropriate property caused by the excitation. For example, if the perturbation is an electric field then the difference in the molecular dipole moment between the ground and excited states can be evaluated.

2.3.1 SF-TDDFT gradients

The derivative of Eq. 29 with respect to a real perturbation is

$$\omega^{\xi} = \sum_{\sigma} \int \rho_{\sigma}^{P(\xi)} \left(T + V_{ext} + V_C + V_{\sigma}^{xc}\right) + \sum_{\sigma} \int \left(V_C^P \rho_{\sigma}^{(\xi)} + V_{ext}^{\xi} \rho_{\sigma}^P\right) + \sum_{\sigma\tau} \int \rho_{\sigma}^P f_{\sigma,\tau}^{xc,FULL} \rho_{\tau}^{(\xi)} + \sum_{\sigma\tau} \int \rho_{\sigma}^{(X+Y)(\xi)} f_{SF,\sigma\tau}^{xc,ALDA} \rho_{\tau}^{(X+Y)} + \sum_{\sigma\tau\upsilon} \int \rho_{\sigma}^{(X+Y)} \rho_{\tau}^{(X+Y)} \rho_{\upsilon}^{(\xi)} g_{SF,\sigma\tau\upsilon}^{xc,ALDA} - \sum_{\mu\nu\sigma} S_{\mu\nu}^{(\xi)} W_{\mu\nu\sigma}^{SF} \quad (51)$$

This equation is very similar to Eq. 31, but it must be kept in mind that ρ^P and ρ^{X+Y} now correspond to spin-flip excitations. The spin-flip forms of the P and W matrices and the R-vector are given in the "Appendix".

The spin-flip form of the third-order derivative of the exchange-correlation functional now has the form

$$g_{SF,\sigma\tau\upsilon}^{xc,ALDA} = \delta_{\sigma\tau} \left(\frac{1}{\left(\rho_\alpha - \rho_\beta\right)^2} \frac{\delta(\rho_\beta - \rho_\alpha)}{\delta\rho_\upsilon} \left(\frac{\delta E^{xc}}{\delta\rho_\alpha} - \frac{\delta E^{xc}}{\delta\rho_\beta} \right) + \frac{1}{\left(\rho_\alpha - \rho_\beta\right)} \left(\frac{\delta^2 E^{xc}}{\delta\rho_\upsilon \delta\rho_\alpha} - \frac{\delta^2 E^{xc}}{\delta\rho_\upsilon \delta\rho_\beta} \right) \right). \quad (52)$$

3 Test calculations

3.1 Computational details

Most calculations in this section were performed with a TZ2P basis set [43]. This basis set is triple-ζ in quality for all valence orbitals and at least double-ζ for all core orbitals and includes a $1p1d$ set of polarization functions for H, a $1d1f$ set for Be, B, C, N, O, Si and P and a $1p1f$ polarization set for Sc and Cu. Diffuse functions were added to the basis set for the calculations of the molecules BH, ScO and CH_2O. The diffuse function sets were $1s1p$ for H, B, C and O and $1s1p1d$ for Sc. A fine grid (integration parameter 6.0) was used throughout. Test calculations suggest that the default grid (integration parameter 4.0) would give results of similar quality.

3.2 Comparisons with earlier work

As a first test of the present implementation, several examples from the test set provided by Furche and Ahrichs [8] were investigated. The molecules chosen were BeH, BH, N_2, ScO, CuH, PH_2 and CH_2O. All excited states considered in [8] were included. The adiabatic excitation energies, geometries, vibrational frequencies and, in the cases of BH, ScO and CH_2O, excited state dipole moments were calculated. The properties were evaluated using the LDA (VWN5), BP86 and B3LYP functionals.

Table 1 Calculated adiabatic excitation energies in eV

Mol.	State	Present			Furche and Ahlrichs			Expt
		LDA	BP	B3LYP	LDA	BP	B3LYP	
BeH	$1^2\Pi$	2.37	2.69	2.64	2.35	2.51	2.55	2.48
BH	$1^1\Pi$	2.49	2.82	2.74	2.35	2.49	2.68	2.87
N_2	$1^3\Pi_g$	6.98	7.04	7.13	7.03	6.73	6.98	7.39
	$1^1\Sigma_u^-$	8.28	8.10	7.91	8.27	8.09	7.90	8.45
	$1^1\Pi_g$	8.45	8.48	8.69	8.46	8.39	8.61	8.59
	$1^1\Delta_u$	8.87	8.78	8.58	8.86	8.50	8.36	8.94
ScO	$1^2\Pi$	2.05	2.08	2.02	2.00	1.93	1.95	2.04
CuH	$2^1\Sigma^+$	3.10	3.06	3.34	3.06	2.97	2.99	2.91
PH_2	1^2A_1	2.14	2.62	2.39	2.13	2.40	2.34	2.27
COH_2	$1^1A''$	3.39	3.51	3.66	3.38	3.44	3.60	3.49
	$1^3A''$	2.69	2.80	2.90	2.68	2.54	2.73	3.12

Zero-point energies are included for PH_2 and COH_2. Results labeled "Furche and Ahlrichs" are TDDFT calculation from [8]. Experimental values are from [62] and [63] for the diatomic molecules and from [64] for PH_2 and COH_2

The results of these calculations are summarized in Tables 1, 2, 3, 4.

Only a few comments need be made about these results. For the most part, the present results closely follow those of Furche and Ahlrichs, giving confidence in our implementation. One result should be noted, however. The LDA adiabatic excitation energies are in close agreement with those calculated by Furche and Ahlrichs with a maximum difference of 0.10 eV, and most of the differences being much smaller than this. The differences between our BP and B3LYP energies and those presented by Furche and Ahlrichs are rather larger with a largest difference of 0.35 eV and several other differences of more than 0.10 eV. The deterioration in agreement when going from LDA to more complicated functionals suggests that the observed differences may be due to the ALDA approximation.

3.3 XH_2 diradicals

The relative energies of the lowest singlet and triplet states of CH_2 have been the subject of theoretical investigation for many years (see [44, 45] and references therein). Methylene and the three isovalent molecules NH_2^+, SiH_2 and PH_2^+ each have two valence electrons not involved in bonding. The four lowest energy states of the XH_2 molecules are three singlet states ($2 \times A_1$ and one B_1) and a triplet B_1 state formed from a $(a_1 b_1)^2$ electron configuration. The lowest energy A_1 state is dominated by the $a_1^2 b_1^0$ electron configuration and the triplet is of course described by the $a_1^1 b_1^1$ configuration. It is simple enough to calculate the energy of these two states through a straightforward DFT calculation in combination with the appropriate

Table 2 Calculated excited state structures

Mol.	State	Param.	Present			Furche and Ahlrichs			Expt
			LDA	BP	B3LYP	LDA	BP	B3LYP	
BeH	$1^2\Pi$	r_e	1.34	1.34	1.32	1.34	1.33	1.32	1.33
BH	$1^1\Pi$	r_e	1.23	1.22	1.21	1.23	1.22	1.21	1.22
N_2	$1^3\Pi_g$	r_e	1.20	1.21	1.20	1.20	1.21	1.20	1.21
	$1^1\Sigma_u^-$	r_e	1.27	1.29	1.27	1.27	1.29	1.27	1.28
	$1^1\Pi_g$	r_e	1.21	1.22	1.21	1.21	1.22	1.21	1.22
	$1^1\Delta_u$	r_e	1.27	1.29	1.27	1.27	1.29	1.27	1.27
ScO	$1^2\Pi$	r_e	1.68	1.70	1.70	1.68	1.71	1.70	1.69
CuH	$2^1\Sigma^+$	r_e	1.60	1.63	1.61	1.59	1.62	1.58	1.57
PH_2	1^2A_1	P–H	1.41	1.41	1.40	1.41	1.41	1.40	1.40
		∠HPH	123	123	122	123	122	122	123
COH_2	$1^1A''$	C–O	1.28	1.31	1.29	1.28	1.31	1.29	1.32
		C–H	1.11	1.11	1.09	111	110	109	110
		∠HCH	115	116	117	115	116	117	118
		ϕ	38	39	35	34	33	30	34
	$1^3A''$	C–O	1.28	1.31	1.29	1.28	1.31	1.29	1.31
		C–H	1.11	1.11	1.10	1.12	1.10	1.10	1.08
		∠HCH	111	113	113	111	110	112	122
		ϕ	51	48	48	44	49	45	41

Bond distances are in Å and angles in degrees. Results labeled "Furche and Ahlrichs" are TDDFT calculation from [8]. Experimental values are from [62] and [63] for the diatomic molecules and from [64] for PH_2 and COH_2

Table 3 Calculated excited state vibrational frequencies in cm^{-1}

Mol.	State	Mode	Present			Furche and Ahlrichs			Expt
			LDA	BP	B3LYP	LDA	BP	B3LYP	
BeH	$1^2\Pi$	ω_e	2,079	2,074	2,158	2,083	2,096	2,161	2,089
BH	$1^1\Pi$	ω_e	2,265	2,260	2,396	2,281	2,263	2,406	2,251
N_2	$1^3\Pi_g$	ω_e	1,856	1,787	1,938	1,858	1,767	1,792	1,733
	$1^1\Sigma_u^-$	ω_e	1,536	1,471	1,544	1,541	1,475	1,546	1,530
	$1^1\Pi_g$	ω_e	1,787	1,715	1,740	1789	1,707	1,736	1,694
	$1^1\Delta_u$	ω_e	1,539	1,476	1,417	1,544	1,483	1,576	1,559
ScO	$1^2\Pi$	ω_e	869	845	856	865	837	846	876
CuH	$2^1\Sigma^+$	ω_e	1,538	1,424	1,615	1,541	1,458	1,657	1,698
PH_2	1^2A_1	$\nu_2(a_1)$	918	940	981	919	934	977	951
COH_2	$1^1A''$	$\nu_1(a')$	2,860	2,897	2,982	2,871	2,906	2,987	2,846
		$\nu_2(a')$	1,362	1,286	1,347	1,364	1,289	1,361	1,183
		$\nu_3(a')$	1,194	1,226	1,297	1,194	1,249	1,301	2,393
		$\nu_5(a'')$	2,952	2,925	3,081	2,963	3,008	3,083	2,968
		$\nu_6(a'')$	812	829	892	809	852	890	904
	$1^3A''$	$\nu_2(a')$	1,365	1,287	1,336	1,369	1,251	1,323	1,283

Results labeled "Furche and Ahlrichs" are TDDFT calculation from [8]. Experimental values are from [62] and [63] for the diatomic molecules and from [64] for PH_2 and COH_2

choice of m_s. The energy of the singlet B_1 state can be calculated by a standard TDDFT calculation with the singlet A_1 state as a reference. On the other hand, the second A_1 state is essentially doubly excited with respect to the first A_1 state and therefore cannot be treated by conventional TDDFT. It can be studied by SF-TDDFT if the triplet

Table 4 Calculated excited state dipole moments in Debye

Mol.	State	Present			Furche and Ahlrichs			Expt
		LDA	BP	B3LYP	LDA	BP	B3LYP	
BH	$1^1\Pi$	0.45	0.45	0.34	0.51	0.52	0.49	0.58
ScO	$1^2\Pi$	4.36	4.22	4.81	4.36	4.34	4.88	4.14
COH_2	$1^1A''$	1.62	1.56	1.44	1.63	1.56	1.53	1.57
	$1^3A''$	1.56	1.47	1.38	1.57	1.42	1.41	1.29

Results labeled "Furche and Ahlrichs" are TDDFT calculation from [8]. Experimental values are from [62]

B_1 state is chosen as the Ref. [28]. In fact, all three singlet states of interest can be reached from this reference, and it was found that the Wang-Ziegler formulation of SF-TDDFT was able to reproduce the relative energies of the lowest four states of CH_2, NH_2^+, SiH_2 and PH_2^+ to good accuracy [28]. For reasons that remain unclear, the Shao-Head-Gordon-Krylov form of SF-TDDFT does not do a good job of predicting the relative energies of these four states [26].

The geometries of these species have been optimized previously by configuration interaction (CI)-based methods [44, 46–48]. We have calculated the geometries of CH_2, NH_2^+, SiH_2 and PH_2^+ in their four lowest states. The triplet state was optimized by a standard DFT calculation of the $m_s = 1$ density, while the geometries of the other three states were calculated using the gradients of the excitation energies of the three lowest spin-flip excitations obtained from the triplet reference. The results of these calculations are compared with CI results in Table 5.

The agreement between the SF-TDDFT calculations and the CI results is reasonably good. The largest difference in calculated bond length between the two types of calculation is 0.03 Å, and the largest difference in angle is 8°. The calculated excitation energies are also similar to the CI results and very close to the SF-TDDFT results obtained using the CI geometries [28].

3.4 Bond breaking

DFT methods in combination with standard functionals are unable to accurately describe the breaking of a covalent bond and the separation of the two newly formed radicals to a large distance. The classic example is the H_2 molecule. The potential energy curve predicted by a restricted Kohn–Sham calculation is much too deep, and the method is not size consistent (the limiting energy approached at large bond lengths is not equal to the sum of the energies of two hydrogen atoms calculated at the same level). If an unrestricted calculation is applied instead, the energetic behavior is much better. The predicted depth of the potential well is decreased and is more in line with the correct result. The energy of the system at long bond distances is equal to the sum of the energy of two hydrogen atoms. On the downside, at longer bond lengths, the calculation suffers from a significant amount of spin contamination. As a consequence, a DFT calculation of H_2 at a stretched geometry does not provide a good starting point for a TDDFT calculation. Calculations of excited state potential energy curves of H_2 with conventional TDDFT have produced poor results [49–51].

Table 5 Excitation energies and geometries of the four lowest states of CH_2, NH_2^+, SiH_2 and PH_2^+ calculated with SF-TDDFT and CI calculations

	State	SF-TDDFT			CI		
		T_e[a]	R_e[b]	∠HXH[c]	T_e[a]	R_e[b]	∠HXH[c]
CH_2	X^3B_1	0.0	1.09	138	0.0	1.08	133
	1^1A_1	0.567	1.12	102	0.411	1.11	102
	1^1B_1	1.356	1.09	145	1.450	1.07	142
	2^1A_1	2.642	1.08	165	2.595	1.07	170
NH_2^+	X^3B_1	0.0	1.05	159	0.0	1.03	151
	1^1A_1	1.353	1.07	110	1.281	1.05	108
	1^1B_1	1.846	1.05	168	1.935	1.03	161
	2^1A_1	3.596	1.05	172	3.308	1.03	180
SiH_2	X^1A_1	0.0	1.54	90	0.0	1.51	93
	1^3B_1	0.913	1.50	119	0.871	1.48	118
	1^1B_1	1.759	1.51	121	1.992	1.48	123
	2^1A_1	3.155	1.48	155	3.486	1.46	162
PH_2^+	X^1A_1	0.0	1.45	90	0.0	1.42	93
	1^3B_1	0.687	1.44	123	0.760	1.41	122
	1^1B_1	1.682	1.45	124	2.009	1.42	125
	2^1A_1	3.265	1.44	156	3.686	1.41	160

CI results from [44, 46–48]

[a] in eV

[b] in Å

[c] in degrees

Attempts have been made to improve the performance of TDDFT near the dissociation limit by modifying the TDDFT coupling matrix [50, 51]. Spin-flip methods have been used to deal with similar problems in wave-function-based methods [52, 53] and also with TDDFT [27].

Much like the XH_2 molecules, the dissociation of H_2 can be understood in terms of two orbitals, a bonding orbital ϕ and an anti-bonding orbital ϕ^*. At short bond lengths, both electrons are in ϕ. At dissociation, the wave function is a combination of the $\phi^\alpha\phi^{*\beta}$ and $\phi^\beta\phi^{*\alpha}$ configurations. All three of these configurations can be reached by a spin-flip from a $\phi^\alpha\phi^{*\alpha}$ reference and a SF-TDDFT calculation with the ${}^3\sigma_u^-$ state as a reference is able to describe transitions from this reference to the ground state and many other excited states.

With the availability of SF-TDDFT gradients, it is now possible to extend this approach to more complicated molecules. Here, we consider the breaking of the C–C bond in ethane.

The $CH_3 + CH_3$ radical combination reaction has been studied a number of times, typically focusing on the long-range interaction region with high-level wave-function-based methods [54–59]. DFT methods encounter similar difficulties to those found for H_2 [54]. Restricted calculations produce a well that is much too deep. Unrestricted calculations using the B3LYP functional suffer from a significant amount of spin contamination at long distances but produce a potential energy curve that is fairly close to a CASPT2 curve [54].

The potential energy curves of the reaction $2CH_3 \rightarrow CH_3CH_3$ calculated with standard restricted DFT methods and by SF-TDDFT from the triplet reference in combination with the LDA and BP functionals are compared with the CASPT2 curve in Fig. 1.

The RDFT calculations show the usual behavior. The curves are much too attractive. The long-range behavior is also incorrect. Although the energy is set to be 0.0 kCal mol^{-1} at 5.0 Å, the restricted LDA (RLDA) and restricted BP (RBP) curves are still increasing at that point, while the CASPT2 curve is almost flat. Furthermore, the RLDA and RBP curves are not size consistent. The energy of $2CH_3$ radicals calculated separately differs by 16.9 kCal mol^{-1} (23.4 kCal mol^{-1}) from the energy of the RLDA (RBP) curve at 5.0 Å.

The SF-TDDFT curves are an improvement on the RDFT results. They follow the CASPT2 curve more closely, though they do show significant differences of about 10 kCal mol^{-1} at 2.5 Å. At the longest bond distances, the slope of the SF-TDDFT curves more closely matches that of the CASPT2 curve. The LDA SF-TDDFT calculations

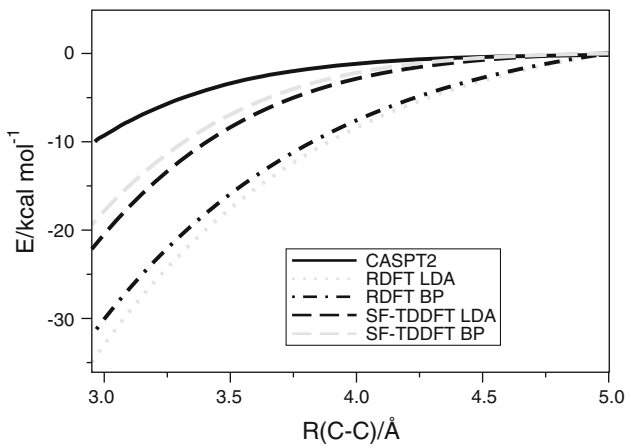

Fig. 1 Energy of ethane as a function of C–C distance calculated by the CASPT2, DFT and SF-TDDFT methods. All curves are shifted so that E(R = 5.0 Å) = 0.0. CASPT2 results are from [54]

are also more size consistent. The LDA SF-TDDFT energy at a C–C separation of 10.0 Å differs by 1.1 kCal mol^{-1} from the energy of two methyl radicals. The BP SF-TDDFT curve has largely the same behavior as the LDA curve with the exception that it is less size consistent. The BP SF-TDDFT energy at a C–C separation of 10.0 Å differs by 18.5 kCal mol^{-1} from the energy of two methyl radicals. We believe that the difference in the size consistency of the two SF calculations is due to the ALDA approximation. The ALDA approximation has two parts. It assumes that the exchange-correlation kernel is frequency independent, and it also assumes that the kernel has the form given by Eq. 18. For an LDA calculation with the VWN5 parametrization of the electron gas as the choice of functional, this second assumption is not an approximation and allows our calculations of the breaking of the C–C bond in ethane to be approximately size consistent.

The SF-TDDFT ground state curves are obviously far from perfectly in agreement with the CASPT2 curves. In order to obtain better agreement, one would have to go beyond linear response [60, 61] and optimize the orbitals for the ground state, as we plan to show in a forthcoming paper. It appears that this approach has potential for describing the energy and gradients of the ground and excited states of medium sized molecules in the dissociative regions of their potential energy surfaces.

4 Concluding remarks

In this paper, we have described the implementation of TDDFT gradients in the ADF program package. The implementation has many similarities to previous implementations, but some different techniques are required because of the use of STOs in ADF.

Van Caillie and Amos and Furche and Ahlrichs make use of the accumulated knowledge of quantum chemical analytical gradients to present very efficient formulations of TDDFT gradients [6, 8]. Gradients are evaluated in terms of integrals over AOs and their derivatives to avoid costly AO to MO transformations. Rather than solving the 3*N* CPKS equations, the single *Z*-vector equation is solved. Similar techniques can be used in ADF. The *Z*-vector approach is used (Eq. 38), and the electron densities and electron density derivatives from Eqs. 31 and 51 are built directly from AOs and AO derivatives. As a result, the computational cost of evaluating the TDDFT gradients is approximately three times the cost of the ground state energy or gradients. About 1/3 of the effort required of a TDDFT gradient calculation is from the solution of the *Z*-vector equation (Eq. 38). The remaining effort is still greater than the ground state gradients because three different densities and density derivatives are needed in

Eq. 31 as opposed to one density and one density derivative in a ground state calculation. In any case, the cost of evaluating the ground state energy, the ground state gradient and the TDDFT gradient is typically less than the effort required to evaluate the TDDFT energy.

SF-TDDFT expands the scope of TDDFT calculations by allowing a greater range of excitations to be treated. With the addition of gradients, the PES of these states can be explored. SF-TDDFT also provides another tool for investigating the more challenging aspects of excited state PES such as seams and conical intersections. Further work is needed to investigate the potential and limitations of SF-TDDFT in this area.

Acknowledgments T.Z. would like to thank the Canadian government for a Canada research chair in theoretical inorganic chemistry. We are grateful to NSERC for funding.

Appendix

The SF-TDDFT gradients equations are similar to those of the standard TDDFT gradients (Eqs. 31–45) with modifications to allow for the different form of the coupling matrix and the fact that all excitations are spin-flips. The overall equation for a SF-TDDFT gradients the spin-flip third-order derivative are given by Eqs. 51 and 52. The other new equations are ($\sigma \neq \sigma'$ in all cases and X and Y are from the spin-flip transition density)

$$\rho^P_\sigma = \sum_{\mu\nu} P^{SF}_{\mu\nu\sigma}\chi_\mu\chi_\nu \tag{53}$$

$$P^{SF} = T^{SF} + Z^{SF} \tag{54}$$

$$T^{SF}_{ij\sigma} = -\frac{1}{2}\sum_a \left((X+Y)_{a\sigma' i\sigma}(X+Y)_{a\sigma' j\sigma} + (X-Y)_{a\sigma' i\sigma}(X-Y)_{a\sigma' j\sigma}\right) \tag{55}$$

$$T^{SF}_{ab\sigma} = \frac{1}{2}\sum_i \left((X+Y)_{a\sigma i\sigma'}(X+Y)_{b\sigma'} + (X-Y)_{a\sigma'}(X-Y)_{b\sigma i\sigma'}\right) \tag{56}$$

$$T^{SF}_{ai\sigma} = T^{SF}_{ia\sigma} = 0 \tag{57}$$

$$Z^{SF}_{ab\sigma} = Z^{SF}_{ij\sigma} = 0 \tag{58}$$

$$(\mathrm{A}+\mathrm{B})Z^{SF} = R^{SF} \tag{59}$$

$$\begin{aligned} R^{SF}_{ai\sigma} = &\sum_b (X+Y)_{b\sigma' i\sigma} H^+_{a\sigma b\sigma'}[X+Y] \\ &+ \sum_j (X+Y)_{a\sigma j\sigma'} H^+_{i\sigma j\sigma'}[X+Y] \\ &+ H^+_{a\sigma i\sigma}\left[T^{SF}\right] \\ &+ 2\sum_{\tau\upsilon}\int \phi_{a\sigma}\phi_{i\sigma}\rho^{X+Y}_\tau \rho^{X+Y}_\upsilon g^{xc,ALDA}_{SF,\sigma\tau\upsilon} \end{aligned} \tag{60}$$

where

$$H^+_{p\sigma q\tau}[M] = 2\int \phi_{p\sigma}\phi_{q\tau}\left(c_{SF}V^M_C + \sum_\upsilon f^{xc}_{\sigma\upsilon}\rho^M_\upsilon\right)M_{rs\sigma} \tag{61}$$

Here the full kernel is needed and $c_{SF} = 1$ when $M = T^{SF}$, P^{SF} and the SF-ALDA kernel and $c_{SF} = 0$ are required when $M = X + Y$.

$$\begin{aligned} W^{SF}_{ij\sigma} = &\sum_a \omega\Big\{\left((X+Y)_{a\sigma' i\sigma}(X-Y)_{a\sigma' j\sigma}\right. \\ &+ (X-Y)_{a\sigma' i\sigma}(X+Y)_{a\sigma' j\sigma}) \\ &- \sum_a \varepsilon_{a\sigma'}\left((X+Y)_{a\sigma' j\sigma}(X+Y)_{a\sigma' i\sigma}\right. \\ &\left.+(X-Y)_{a\sigma' j\sigma}(X-Y)_{a\sigma' i\sigma}\right)\Big\} \\ &+ H^+_{ij\sigma}[P] + 2\sum_{\tau\upsilon}\int \phi_{i\sigma}\phi_{j\sigma}\rho^{(X+Y)}_\tau \rho^{(X+Y)}_\upsilon g^{xc,ALDA}_{SF,\sigma\tau\upsilon} \end{aligned} \tag{62}$$

$$\begin{aligned} W^{SF}_{ab\sigma} = &\sum_i \omega\Big\{\left((X+Y)_{a\sigma i\sigma'}(X-Y)_{b\sigma i\sigma'}\right. \\ &\left.+ (X-Y)_{a\sigma i\sigma'}(X+Y)_{b\sigma i\sigma'}\right) \\ &+ \sum_i \varepsilon_{i\sigma'}\left((X+Y)_{a\sigma i\sigma'}(X+Y)_{b\sigma i\sigma'}\right. \\ &\left.+ (X-Y)_{a\sigma i\sigma'}(X-Y)_{b\sigma i\sigma'}\right)\Big\} \end{aligned} \tag{63}$$

$$W^{SF}_{ia\sigma} = Z^{SF}_{ai\sigma}\varepsilon_{i\sigma} + \sum_j (X+Y)_{a\sigma j\sigma'} H^+_{j\sigma' i\sigma}[X+Y]. \tag{64}$$

References

1. Gross EKU, Dobson JF, Petersilka M (1996) In: Topics in current chemistry, vol 181. Springer, Berlin, pp 81–172
2. Casida ME (1995) In: Chang DP (ed) Recent advances in density functional theory, vol 1. World Scientific, Singapore, pp 155–192
3. Jamorski C, Casida M, Salahub D (1996) J Chem Phys 104:5134
4. Bauernschmitt R, Ahlrichs R (1996) Chem Phys Lett 256:454
5. Marques MAL, Ullrich CA, Nogueira F, Rubio A, Burke K, Gross EKU (eds) (2006) Time-dependent density functional theory. Lecture notes in physics, vol 706. Springer, Berlin
6. Van Caillie C, Amos RD (1999) Chem Phys Lett 308:249
7. Van Caillie C, Amos RD (2000) Chem Phys Lett 317:159
8. Furche F, Ahlrichs R (2002) J Chem Phys 117:7433
9. Furche F, Ahlrichs R (2002) J Chem Phys 121:12772
10. Rappoport D, Furche F (2006) In: Time-dependent density functional theory, Lecture notes in physics, vol 706. Springer, Berlin, pp 337–357
11. Seth M, Ziegler T (2007) J Chem Phys 127:134108
12. Seth M, Ziegler T (2010) In: van Eldik R, Harvey J (eds) advances in inorganic chemistry, vol 62. Academic Press, San Diego
13. Levine BG, Ko C, Quennevile J, Martinez TJ (2006) Mol Phys 104:1039
14. Tapavicza E, Tavernelli I, Rothlisberger U, Filipi C, Casida ME (2008) J Chem Phys 129:124108
15. Tavernelli I, Tapavicza E, Rothlisberger U (2009) J Chem Phys 130:124107

16. Minezawa N, Gordon MS (2009) J Phys Chem A Lett 113:12749
17. Send R, Furche F (2010) J Chem Phys 132:044107
18. Hutter J (2003) J Chem Phys 118:3928
19. Hutter J (2006) In: Time-dependent density functional theory. Lecture notes in physics, vol 706. Springer, Berlin, pp 217–226
20. Baerends EJ, Ellis DE, Ros P (1973) Chem Phys 2:41
21. Watson MA, Handy NC, Cohen AJ (2003) J Chem Phys 119:6475
22. Watson MA, Handy NC, Cohen AJ, Helgaker T (2004) J Chem Phys 120:7252
23. Krykunov M, Ziegler T, Van Lenthe E (2009) Int J Quantum Chem 109:1676
24. van Gisbergen SJA, Kootstra F, Schipper PRT, Gritsenko OV, Snijders JG, Baerends EJ (1998) Phys Rev A 57:25568
25. van Gisbergen SJA, Groeneveld JA, Rosa A, Snijders JG, Baerends EJ (1999) J Phys Chem A 103:6835
26. Shao Y, Head-Gordon M, Krylov AI (2003) J Chem Phys 118: 4807
27. Wang F, Ziegler T (2004) J Chem Phys 121:12191
28. Wang F, Ziegler T (2005) J Chem Phys 122:074109
29. Eshring H, Servedio VDP (1999) J Comput Chem 20:23
30. van Wullen C (2002) J Comput Chem 23:227
31. Wang F, Liu W (2003) J Chin Chem Soc (Taipei) 50:597
32. Baerends EJ, Autschbach J, Bashford D, Bérces A, Bickelhaupt FM, Bo C, Boerrigter PM, Cavallo L, Chong DP, Deng L, Dickson RM, Ellis DE, Fan L, Fischer TH, Fonseca Guerra C, Ghysels A, Giammona A, van Gisbergen SJA, Götz AW, Groeneveld JA, Gritsenko OV, Grüning M, Harris FE, van der Hoek P, Jacob CR, Jacobsen H, Jensen L, van Kessel G, Koostra F, Krykunov M, van Lenthe E, McCormack DA, Michalak A, Mitoraj M, Neugebauer J, Nicu VP, Noodleman L, Osinga VP, Patchkovskii S, Philipsen PHT, Post D, Pye CC, Ravenek W, Rodriguez JI, Ros P, Schipper PRT, Schreckenbach G, Seth M, Snijders JG, Sóla M, Swart M, Swerhone D, te Velde G, Vernooijs P, Versluis L, Visscher L, Visser O, Wang F, Wesolowski TA, van Wezenbeek E, Wiesenekker G, Wolff SK, Woo TK, Yakovlev AL, Ziegler T (2009) ADF2009.01, SCM, Theoretical Chemistry, Vrije Universiteit, Amsterdam, The Netherlands, http://www.scm.com
33. te Velde G, Bickelhaupt FM, Baerends EJ, Fonseca Guerra C, van Gisbergen SJA, Snijders JG, Ziegler T (2001) J Comput Chem 22:931
34. Fonseca Guerra C, Snijders JG, te Velde G, Baerends EJ (1998) Theor Chim Acta 99:391
35. Boerrigter PM, te Velde G, Baerends EJ (1988) Int J Quantum Chem 33
36. te Velde G, Baerends EJ (1992) J Comput Phys 99:84
37. Jacobsen H, Bérces A, Swerhome D, Ziegler T (1997) Comput Phys Commun 100:263
38. Wolff SK (2005) Int J Quantum Chem 104:645
39. Vosko SH, Wilk L, Nusair M (1980) Can J Phys 58:1200
40. van Gisbergen SJA, Snijders JG, Baerends EJ (1999) Comput Phys Commun 118:119
41. Handy NC, Schaefer IHF (1984) J Chem Phys 81:5031
42. Scalmani G, Frisch MJ, Mennucci B, Tomasi J, Cammi R, Barone V (2006) J Chem Phys 124:094107
43. Van Lenthe E, Baerends EJ (2003) J Comput Chem 24:1142
44. Sherrill CD, Leininger ML, Van Huis TJ, Schaefer HF III (1998) J Chem Phys 108:1040
45. Slipchenko LV, Krylov AI (2002) J Chem Phys 117:4694
46. Stefens JC, Yamaguchi Y, Sherrill CD, Schaefer HF III (1998) J Phys Chem 102:3999
47. Yamaguchi Y, Van Huis TJ, Sherrill CD, Schaefer HF III (1997) Theor Chim Acta 97:341
48. Van Huis TJ, Yamaguchi Y, Sherrill CD, Schaefer HF III (1997) J Phys Chem 101:6955
49. Cai ZL, Reimers JR (2000) J Chem Phys 112:527
50. Casida ME, Gutierrez F, Guan J, Gadea FX, Salahub D, Daudey JP (2000) J Chem Phys 113:7062
51. Gritsenko OV, van Gisbergen SJA, Görling A, Baerends EJ (2000) J Chem Phys 113:8478
52. Krylov AI (2001) Chem Phys Lett 338:375
53. Krylov AI (2001) Chem Phys Lett 350:522
54. Garding LB, Klippenstein SJ, Jasper AW (2007) Phys Chem Chem Phys 9:4055
55. Klippenstein SJ, Georgievskii Y, Harding LB (2006) Phys Chem Chem Phys 8:1133
56. Klippenstein SJ, Harding LB (1999) J Phys Chem A 103:9388
57. Naroźnik M (1998) J Chem Soc Faraday Trans 94:2531
58. Robertson SH, Wardlaw DM, Hirst DM (1993) J Chem Phys 99:7748
59. Darvesh KV, Boyd RJ, Pacey PD (1989) J Phys Chem 93:4772
60. Ziegler T, Seth M, Krykunov M, Autschbach J (2008) J Chem Phys 129:184114
61. Ziegler T, Seth M, Krykunov M, Autschbach J, Wang F (2009) J Chem Phys 130:154102
62. Huber KP, Herzberg G (1979) Molecular spectra and molecular structure, vol IV. Van Nostrand Reinhold, New York
63. Bauschlicher CW, Langhoff SR (1986) J Chem Phys 85:5936
64. Herzberg G (1966) Molecular spectra and molecular structure, vol II. Van Nostrand Reinhold, New York